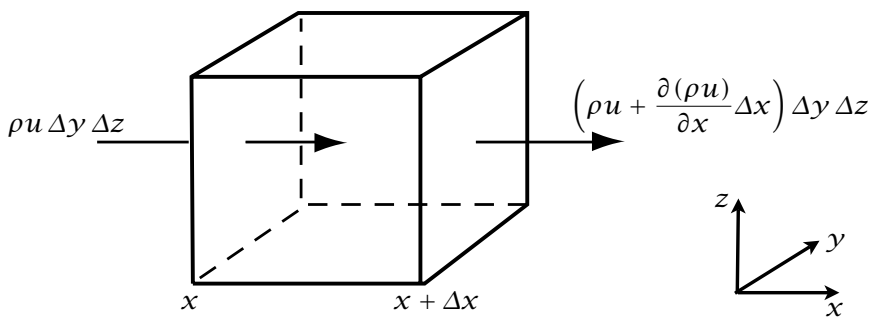

Fig. 1.1 Mass conservation in an Eulerian cuboid control volume.

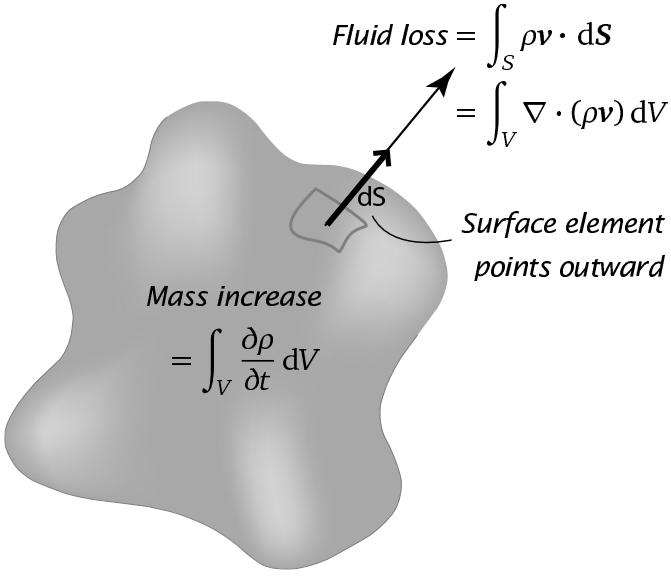

Fig. 1.2 Mass conservation in an arbitrary Eulerian control volume V bounded by a surface S. The mass gain, $\int_V (\partial \rho / \partial t)\, \mathrm{d}V$ is equal to the mass flowing into the volume, $-\int_S (\rho \boldsymbol{v}) \cdot \mathrm{d}\boldsymbol{S} = -\int_V \nabla \cdot (\rho \boldsymbol{v})\, \mathrm{d}V$.

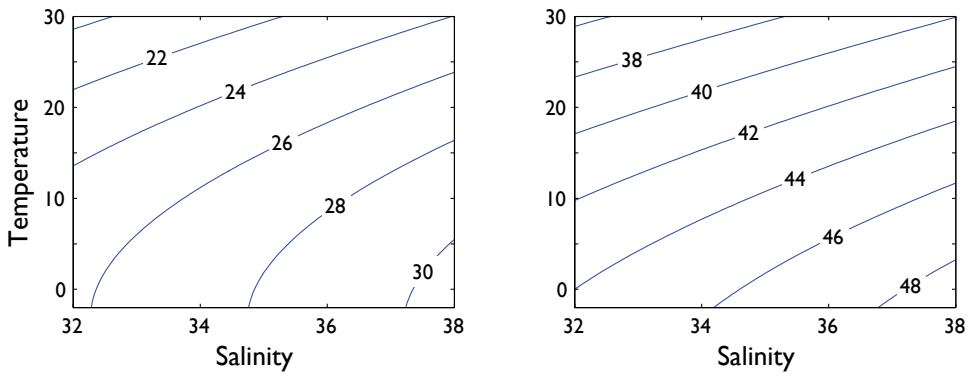

Fig. 1.3 A temperature–salinity diagram for seawater, calculated using an accurate empirical equation of state. Contours are (density $-\,1000$) kg m^{-3}, and the temperature is potential temperature, which in the deep ocean may be less than *in situ* temperature by a degree or so (see Fig. 1.4). Left panel: at sea-level ($p = 10^5$ Pa $= 1000$ mb). Right panel: at $p = 4 \times 10^7$ Pa, a depth of about 4 km. Note that in both cases the contours are slightly convex.

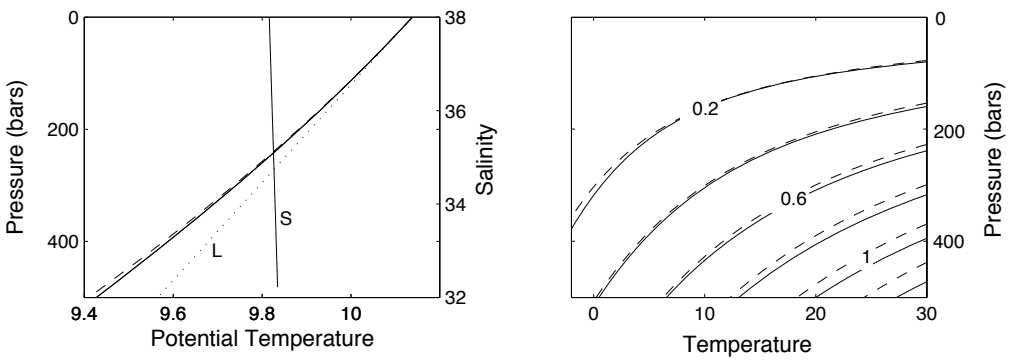

Fig. 1.4 Examples of the variation of potential temperature of seawater with pressure, temperature and salinity. Left panel: the sloping lines show potential temperature as a function of pressure at fixed salinity ($S = 35$ psu) and temperature (13.36°C). The solid line is computed using an accurate, empirical equation of state, the almost-coincident dashed line uses the simpler expression (1.153) and the dotted line (labelled L) uses the linear expression (1.154c). The near vertical solid line, labelled S, shows the variation of potential temperature with salinity at fixed temperature and pressure. Right panel: Contours of the difference between temperature and potential temperature, $(T - \theta)$ in the pressure–temperature plane, for $S = 35$ psu. The solid lines use an accurate empirical formula, and the dashed lines use (1.153). The simpler equation can be improved locally, but not globally, by tuning the coefficients. (100 bars of pressure (10^7 Pa or 10 MPa) is approximately 1 km depth.)

From Vallis (2006)

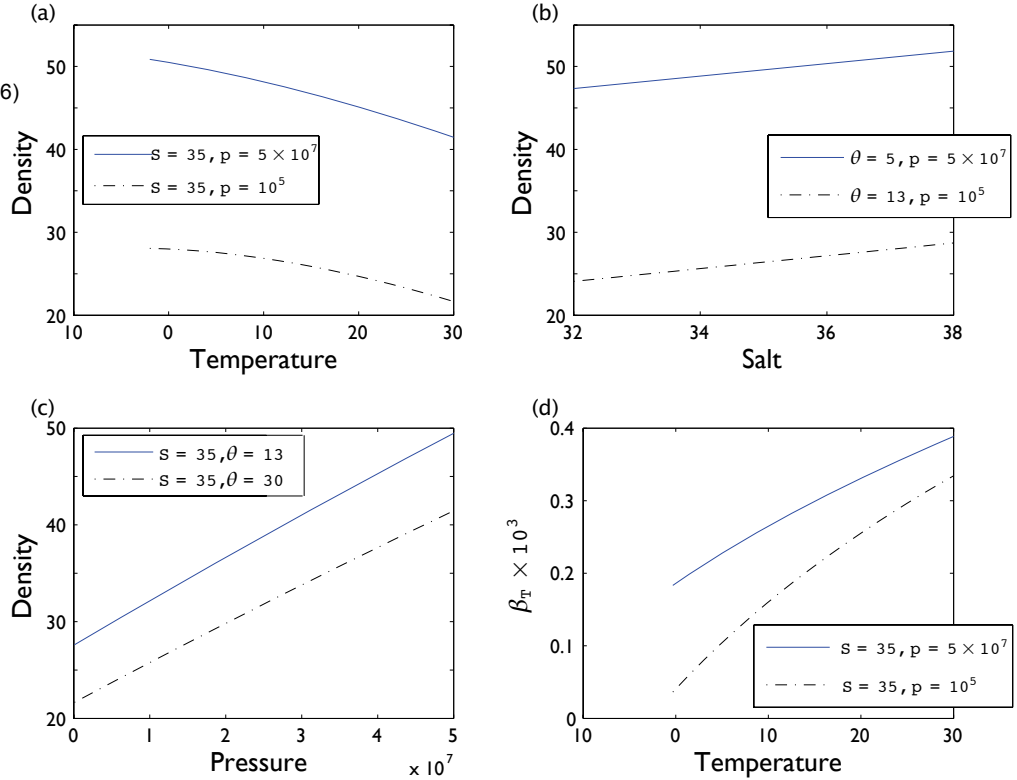

Fig. 1.5 Examples of the variation of density of seawater (minus $1000\,\mathrm{kg\,m^{-3}}$) with (a) potential temperature (°C); (b) salt (psu); and (c) pressure (Pa), for seawater. Panel (d), shows the thermal expansion coefficient, $\widehat{\beta}_T = -\rho^{-1}(\partial\rho/\partial T)_{p,S}\,\mathrm{K}^{-1}$, for each of the two curves in panel (a).

From Vallis (2006)

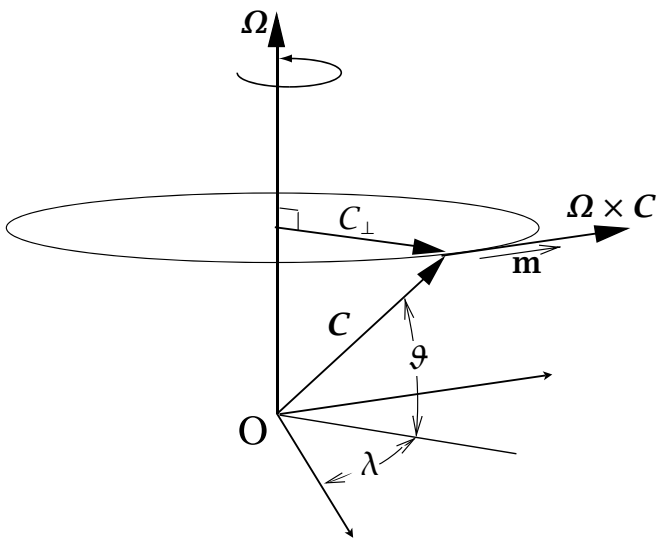

Fig. 2.1 A vector $\boldsymbol{C}$ rotating at an angular velocity $\boldsymbol{\Omega}$. It appears to be a constant vector in the rotating frame, whereas in the inertial frame it evolves according to $(\mathrm{d}\boldsymbol{C}/\mathrm{d}t)_I = \boldsymbol{\Omega} \times \boldsymbol{C}$.

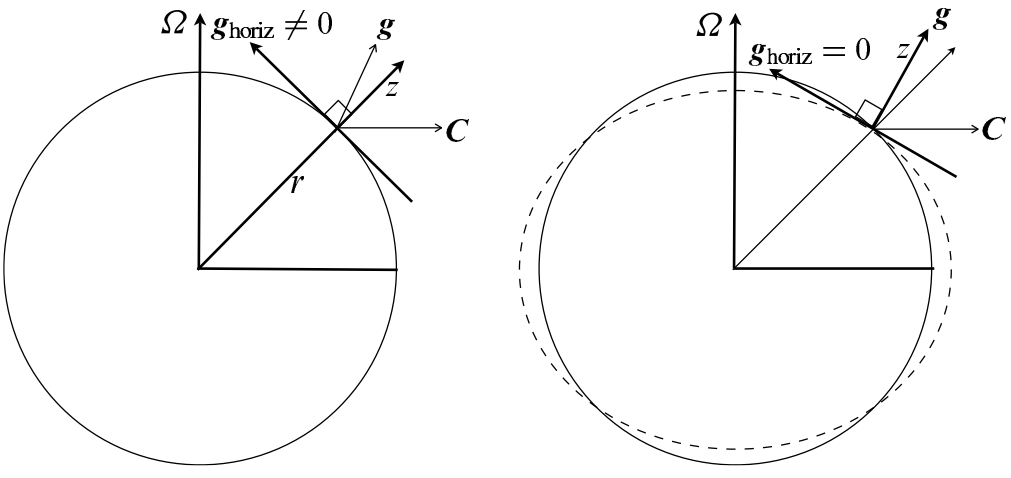

Fig. 2.2 Left: directions of forces and coordinates in true spherical geometry. $\boldsymbol{g}$ is the effective gravity (including the centrifugal force, $\boldsymbol{C}$) and its horizontal component is evidently non-zero. Right: a modified coordinate system, in which the vertical direction is defined by the direction of $\boldsymbol{g}$, and so the horizontal component of $\boldsymbol{g}$ is identically zero. The dashed line schematically indicates a surface of constant geopotential. The differences between the direction of $\boldsymbol{g}$ and the direction of the radial coordinate, and between the sphere and the geopotential surface, are much exaggerated and in reality are similar to the thickness of the lines themselves.

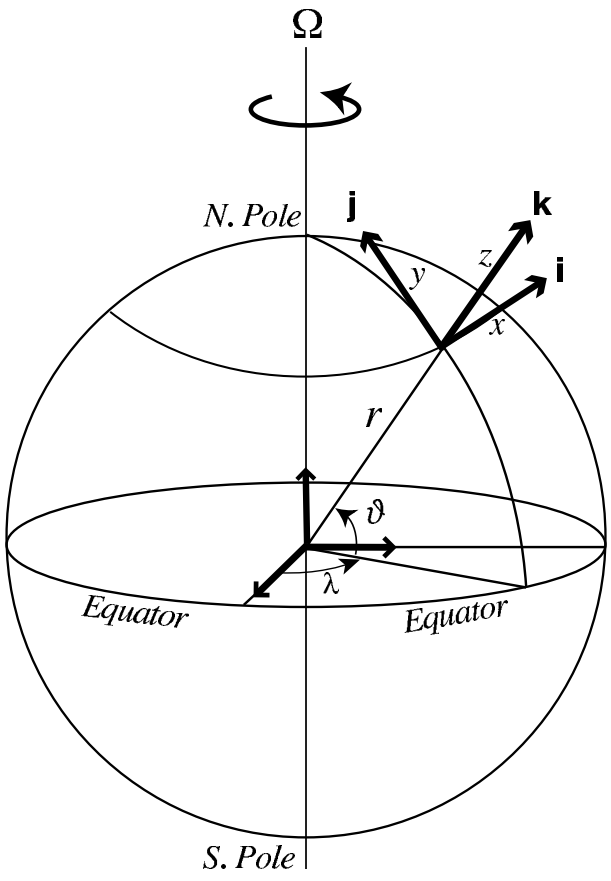

Fig. 2.3 The spherical coordinate system. The orthogonal unit vectors $\mathbf{i}$, $\mathbf{j}$ and $\mathbf{k}$ point in the direction of increasing longitude λ, latitude ϑ, and altitude z. Locally, one may apply a Cartesian system with variables x, y and z measuring distances along $\mathbf{i}$, $\mathbf{j}$ and $\mathbf{k}$.

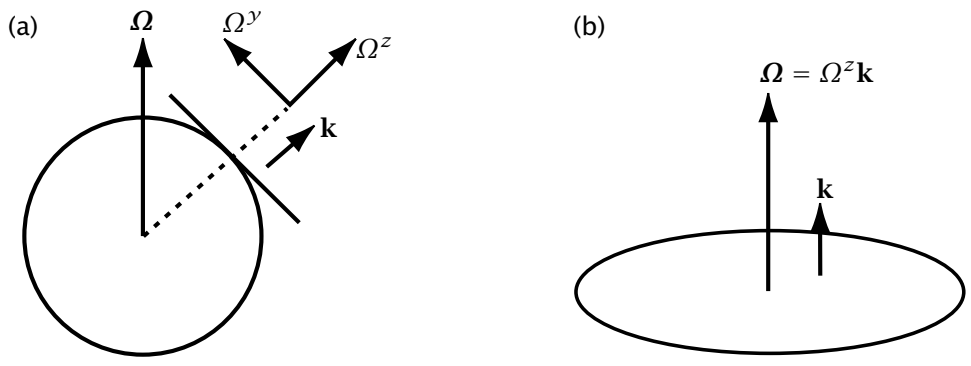

Fig. 2.4 (a) On the sphere the rotation vector $\boldsymbol{\Omega}$ can be decomposed into two components, one in the local vertical and one in the local horizontal, pointing toward the pole. That is, $\boldsymbol{\Omega} = \Omega_y\mathbf{j} + \Omega_z\mathbf{k}$ where $\Omega_y = \Omega\cos\vartheta$ and $\Omega_z = \Omega\sin\vartheta$. In geophysical fluid dynamics, the rotation vector in the local vertical is often the more important component in the horizontal momentum equations. On a rotating disk, (b), the rotation vector $\boldsymbol{\Omega}$ is parallel to the local vertical $\mathbf{k}$.

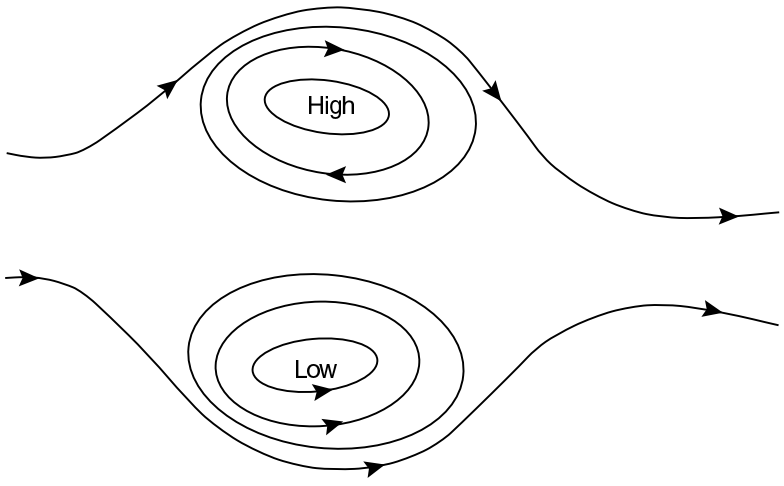

Fig. 2.5 Schematic of geostrophic flow with a positive value of the Coriolis parameter f. Flow is parallel to the lines of constant pressure (isobars). Cyclonic flow is anticlockwise around a low pressure region and anticyclonic flow is clockwise around a high. If f were negative, as in the Southern Hemisphere, (anti)cyclonic flow would be (anti)clockwise.

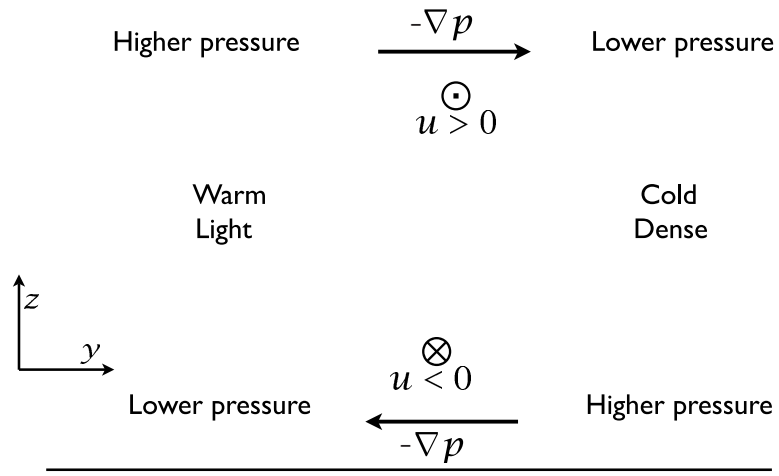

Fig. 2.6 The mechanism of thermal wind. A cold fluid is denser than a warm fluid, so by hydrostasy the vertical pressure gradient is greater where the fluid is cold. Thus, the pressure gradients form as shown, where 'higher' and 'lower' mean relative to the average at that height. The horizontal pressure gradients are balanced by the Coriolis force, producing (for $f > 0$) the horizontal winds shown ($\otimes$ into the paper, and $\odot$ out of the paper). Only the wind *shear* is given by the thermal wind.

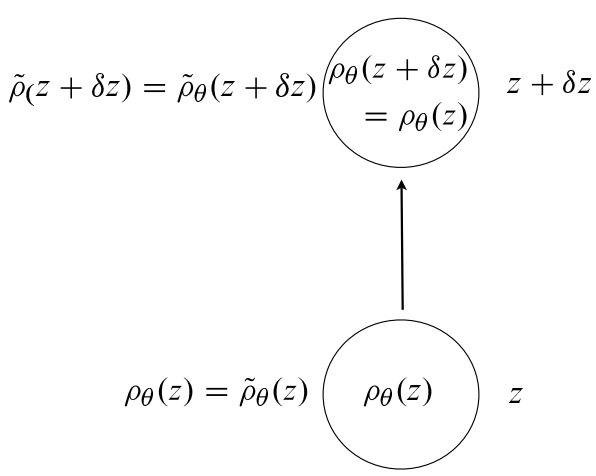

Fig. 2.7 A parcel is adiabatically displaced upward from level z to $z + \delta z$. If the resulting density difference, $\delta\rho$, between the parcel and its new surroundings is positive the displacement is stable, and conversely. If $\tilde{\rho}$ is the environmental values, and ρ_θ is potential density, we see that $\delta\rho = \tilde{\rho}_\theta(z) - \tilde{\rho}_\theta(z + \delta z)$.

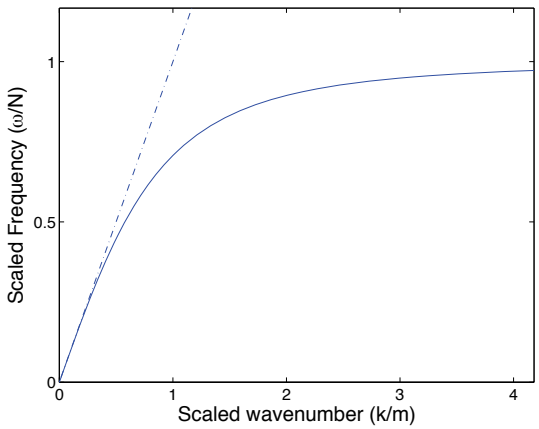

Fig. 2.8 Scaled frequency, ω/N, plotted as a function of scaled horizontal wavenumber, k/m, using the full dispersion relation of (2.248) (solid line, asymptoting to unit value for large k/m) and with the hydrostatic dispersion relation (2.252) (dashed line, tending to ∞ for large k/m).

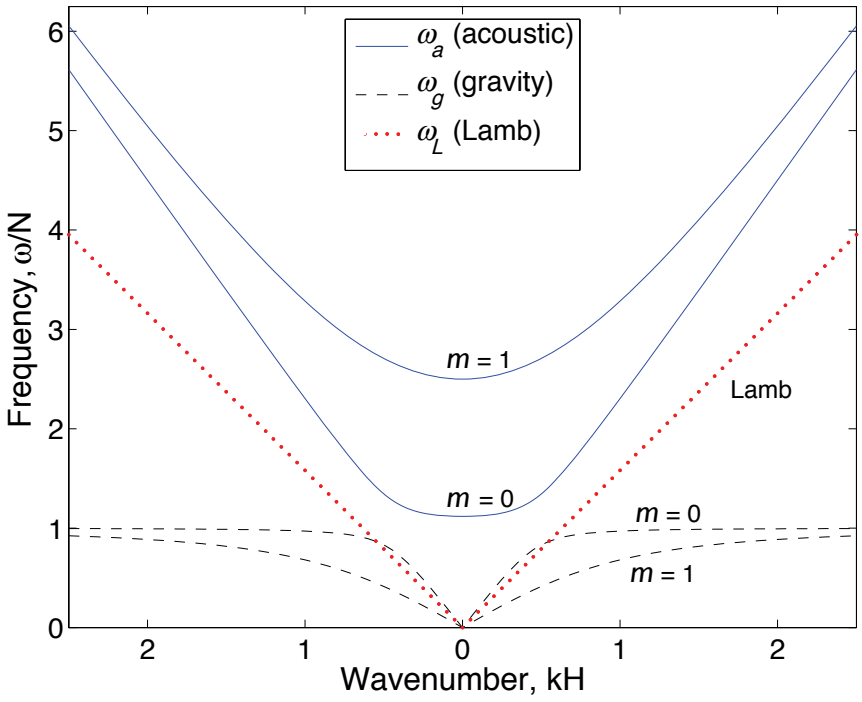

Fig. 2.9 Dispersion diagram for acoustic gravity waves in an isothermal atmosphere, calculated using (2.261). The frequency is given in units of the the buoyancy frequency N, and the wavenumbers are non-dimensionalized by the inverse of the scale height, H. The solid curves indicate acoustic waves, whose frequency is always higher than that of the corresponding Lamb wave at the same wavenumber (i.e., ck), and of the base acoustic frequency $\approx 1.12N$. The dashed curves indicate internal gravity waves, whose frequency asymptotes to N at small horizontal scales.

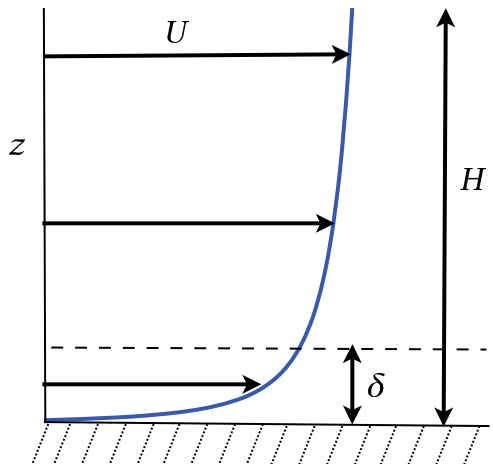

Fig. 2.10 An idealized boundary layer. The values of a field, such as velocity, U, may vary rapidly in a boundary in order to satisfy the boundary conditions at a rigid surface. The parameter δ is a measure of the boundary layer thickness, and H is a typical scale of variation away from the boundary.

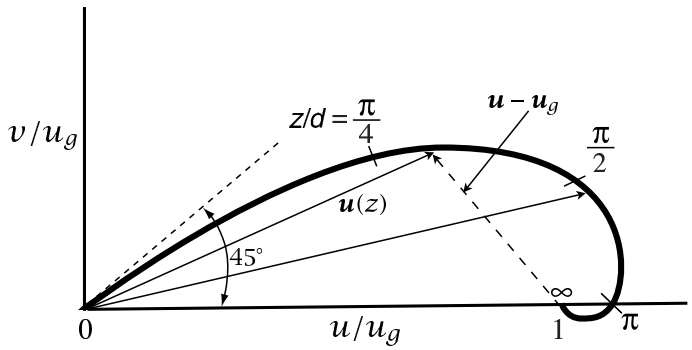

Fig. 2.11 The idealized Ekman layer solution in the lower atmosphere, plotted as a hodograph of the wind components: the arrows show the velocity vectors at a particular heights, and the curve traces out the continuous variation of the velocity. The values on the curve are of the non-dimensional variable z/d, where $d = (2A/f)^{1/2}$, and v_g is chosen to be zero.

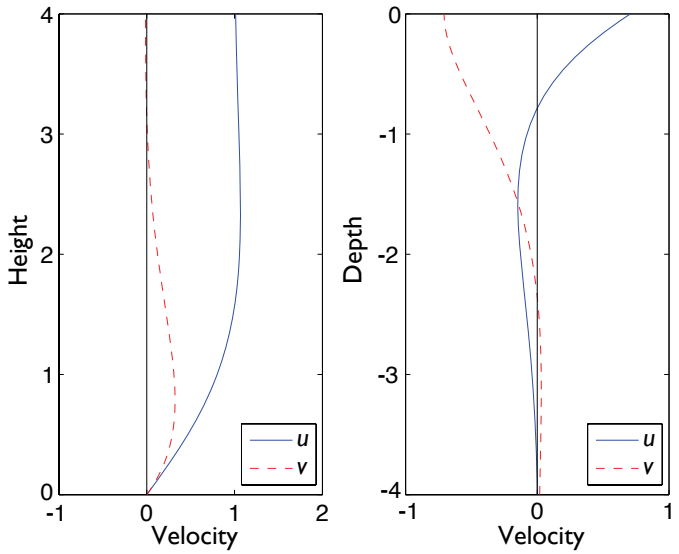

Fig. 2.12 Solutions for a bottom Ekman layer with a given flow in the fluid interior (left), and for a top Ekman layer with a given surface stress (right), both with $d = 1$. On the left we have $u_g = 1$, $v_g = 0$. On the right we have $u_g = v_g = 0$, $\tilde{\tau}_y = 0$ and $\sqrt{2}\tilde{\tau}_x/(fd) = 1$.

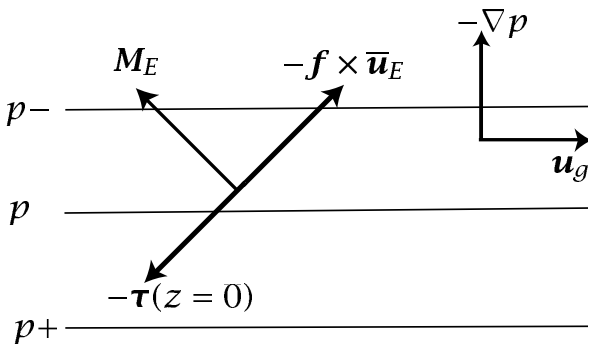

Fig. 2.13 A bottom Ekman layer, generated from an eastward geostrophic flow above it. An overbar denotes a vertical integral over the Ekman layer, so that $-\boldsymbol{f}\times\overline{\boldsymbol{u}}_E$ is the Coriolis force on the vertically integrated Ekman velocity. $\boldsymbol{M}_E$ is the frictionally induced boundary layer transport, and $\boldsymbol{\tau}$ is the stress.

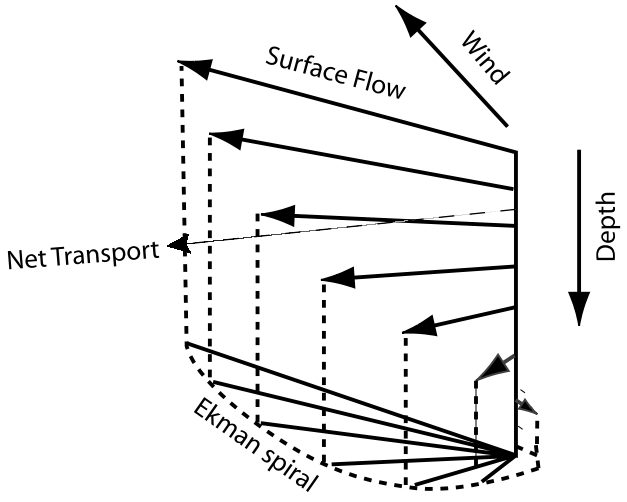

Fig. 2.14 An idealized Ekman spiral in a southern hemisphere ocean, driven by an imposed wind stress. A northern hemisphere spiral would be the reflection of this about the vertical axis. Such a clean spiral is rarely observed in the real ocean. The net transport is at right angles to the wind, independent of the detailed form of the friction. The angle of the surface flow is 45° to the wind only for a Newtonian viscosity.

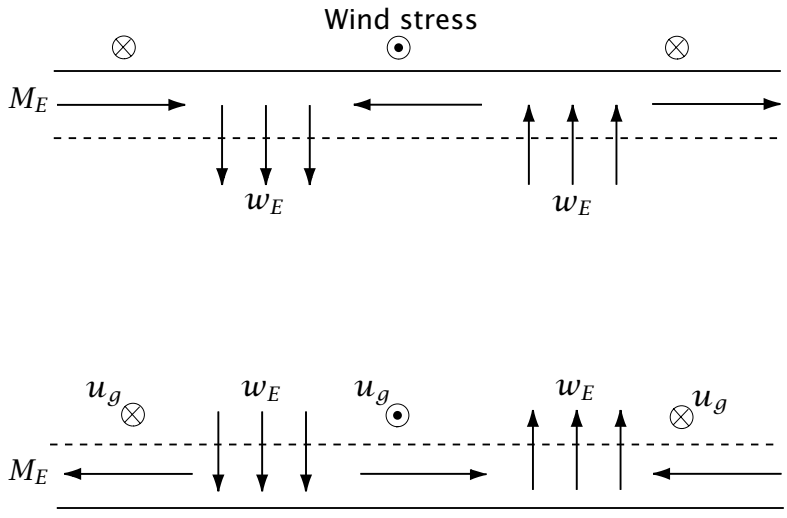

Fig. 2.15 Upper and lower Ekman layers. The upper Ekman layer in the ocean is primarily driven by an imposed wind stress, whereas the lower Ekman layer in the atmosphere or ocean largely results from the interaction of interior geostrophic velocity and a rigid lower surface. The upper part of figure shows the vertical Ekman 'pumping' velocities that result from the given wind stress, and the lower part of the figure shows the Ekman pumping velocities given the interior geostrophic flow.

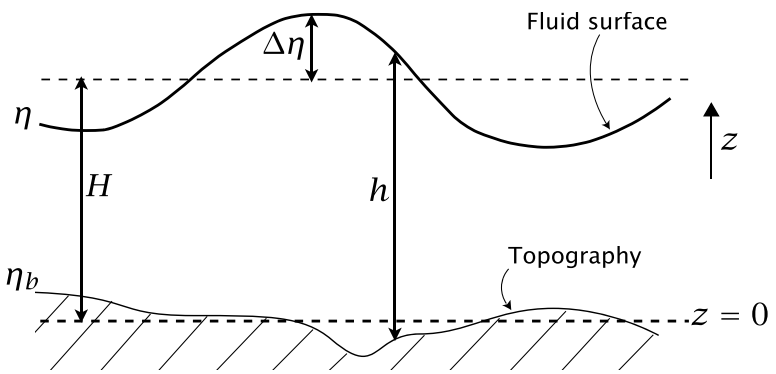

Fig. 3.1 A shallow water system. h is the thickness of a water column, H its mean thickness, η the height of the free surface and η_b is the height of the lower, rigid, surface, above some arbitrary origin, typically chosen such that the average of η_b is zero. $\Delta\eta$ is the deviation free surface height, so we have $\eta = \eta_b + h = H + \Delta\eta$.

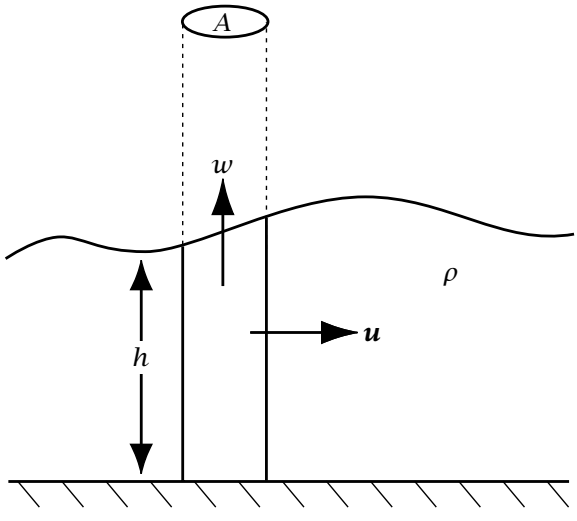

Fig. 3.2 The mass budget for a column of area A in a shallow water system. The fluid leaving the column is $\oint \rho h \boldsymbol{u} \cdot \boldsymbol{n} \, \mathrm{d}l$ where $\boldsymbol{n}$ is the unit vector normal to the boundary of the fluid column. There is a non-zero vertical velocity at the top of the column if the mass convergence into the column is non-zero.

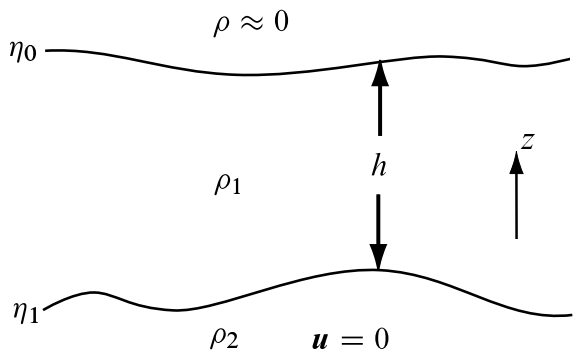

Fig. 3.3 The reduced gravity shallow water system. An active layer lies over a deep, more dense, quiescent layer. In a common variation the upper surface is held flat by a rigid lid, and $\eta_0 = 0$.

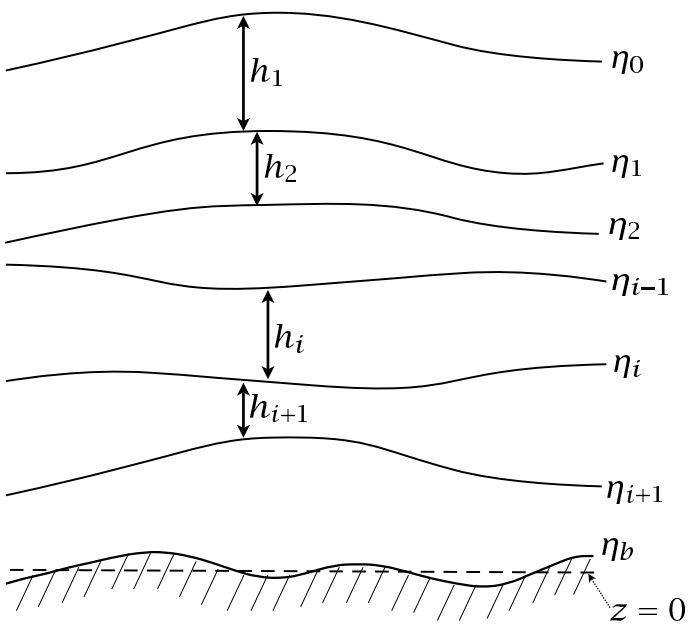

Fig. 3.4 The multi-layer shallow water system. The layers are numbered from the top down. The coordinates of the interfaces are denoted by η, and the layer thicknesses by h, so that $h_i = \eta_i - \eta_{i-1}$.

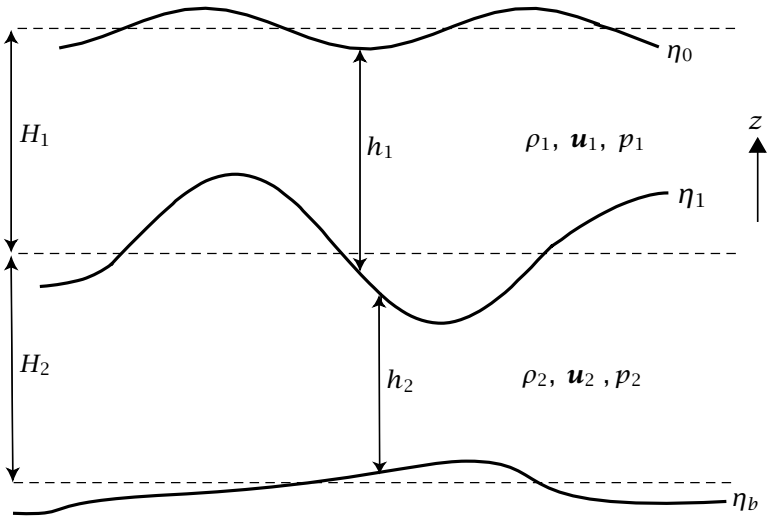

Fig. 3.5 The two-layer shallow water system. A fluid of density ρ_1 lies over a denser fluid of density ρ_2. In the reduced gravity case the lower layer may be arbitrarily thick and is assumed stationary and so has no horizontal pressure gradient. In the 'rigid-lid' approximation the top surface displacement is neglected, but there is then a non-zero pressure gradient induced by the lid.

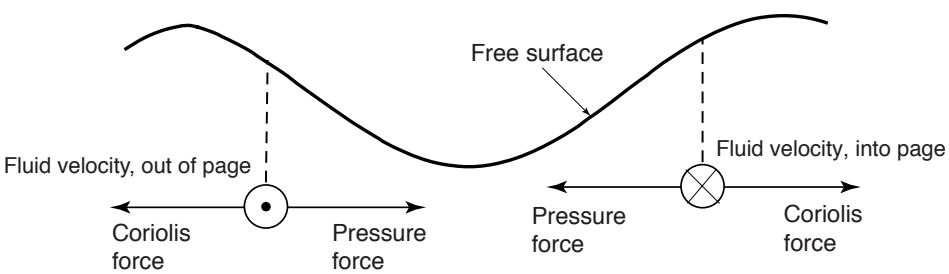

Fig. 3.6 Geostrophic flow in a shallow water system, with a positive value of the Coriolis parameter f, as in the Northern Hemisphere. The pressure force is directed down the gradient of the height field, and this can be balanced by the Coriolis force if the fluid velocity is at right angles to it. If f were negative, the geostrophic flow would be reversed.

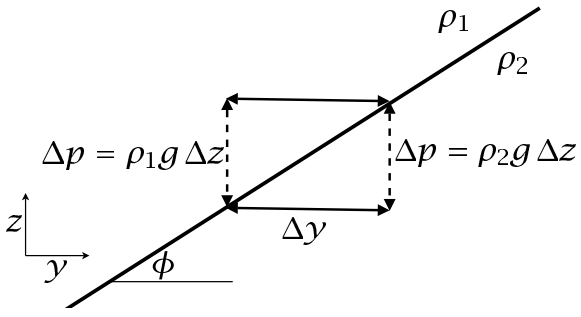

Fig. 3.7 Margules' relation: using hydrostasy, the difference in the horizontal pressure gradient between the upper and the lower layer is given by $-g'\rho_1 s$, where $s = \tan\phi = \Delta z/\Delta y$ is the interface slope and $g' = (\rho_2 - \rho_1)/\rho_1$. Geostrophic balance then gives $f\partial_y(u_1 - u_2) = g's$, which is a special case of (3.60).

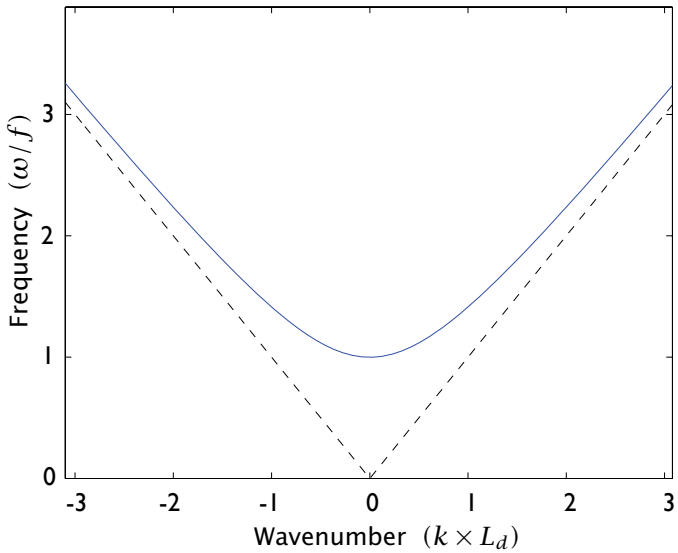

Fig. 3.8 Dispersion relation for Poincaré waves (solid) and non-rotating shallow water waves (dashed). Frequency is scaled by the Coriolis frequency f, and wavenumber by the inverse deformation radius $\sqrt{gH}/f$. For small wavenumbers the frequency is approximately f; for high wavenumbers it asymptotes to that of non-rotating waves.

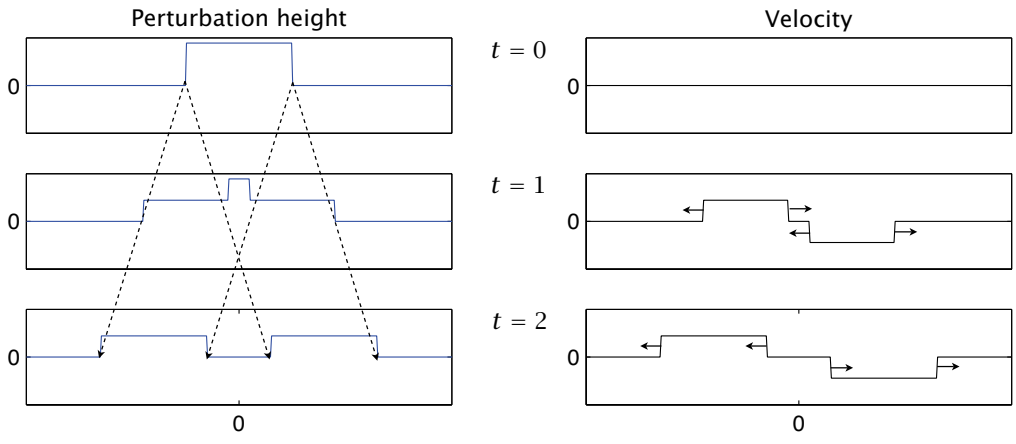

Fig. 3.9 The time development of an initial 'top hat' height disturbance, with zero initial velocity, in non-rotating flow. Fronts propagate in both directions, and the velocity is non-zero between fronts, but ultimately the velocity and height disturbance are radiated away to infinity.

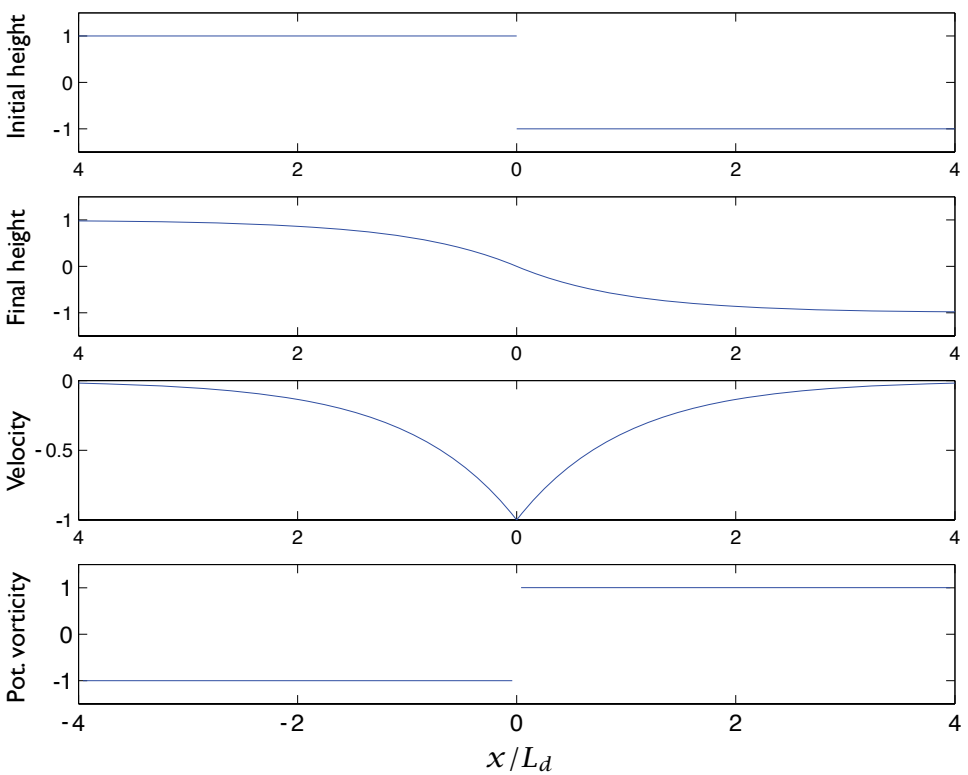

Fig. 3.10 Solutions of a linear geostrophic adjustment problem. Top panel: the initial height field, given by (3.121) with $\eta_0 = 1$. Second panel: equilibrium (final) height field, η given by (3.134) and $\eta = f_0\psi/g$. Third panel: equilibrium geostrophic velocity (normal to the gradient of height field), given by (3.135). Bottom panel: potential vorticity, given by (3.130), and this does note evolve. The distance, x is non-dimensionalized by the deformation radius $L_d = \sqrt{gH}/f_0$, and the velocity by $\eta_0(g/f_0L_d)$. Changes to the initial state occur only within $\mathcal{O}(L_d)$ of the initial discontinuity; and as $x \to \pm\infty$ the initial state is unaltered.

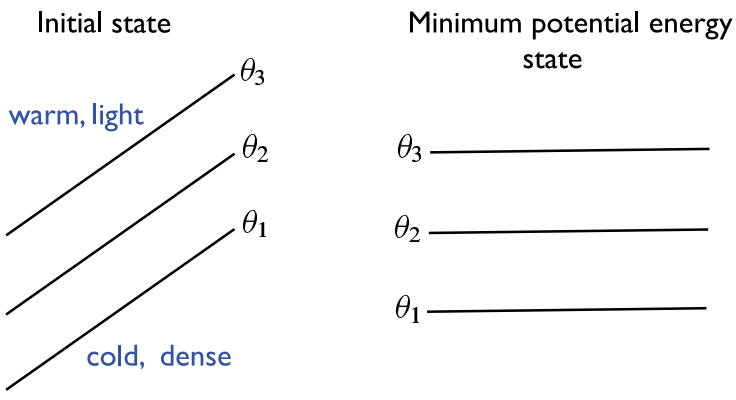

Fig. 3.11 If a stably stratified initial state with sloping isentropes (left) is adiabatically rearranged then the state of minimum potential energy has flat isentropes, as on the right, but the amount of fluid contained between each isentropic surface is unchanged. The difference between the potential energies of the two states is the *available potential energy*.

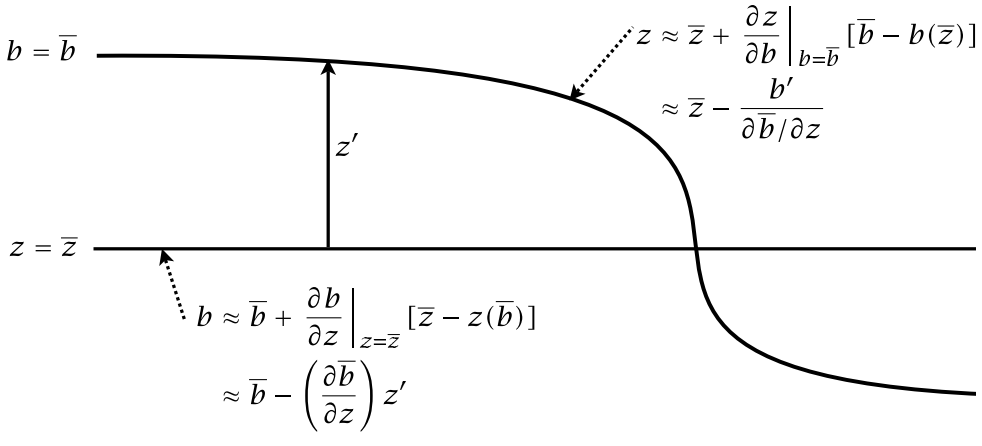

Fig. 3.12 An isopycnal surface, $b = \overline{b}$, and the constant height surface, $z = \overline{z}$. $\overline{z}$ is the height of the isopycnal surface after a rearrangement to a minimum potential energy state, equal to the average height of the isopycnal surface. The values of z on the isopycnal surface, and of b on the constant height surface, can be obtained by the Taylor expansions shown. For an ideal gas in pressure coordinates, replace z by p and b by θ.

From Vallis (2006)

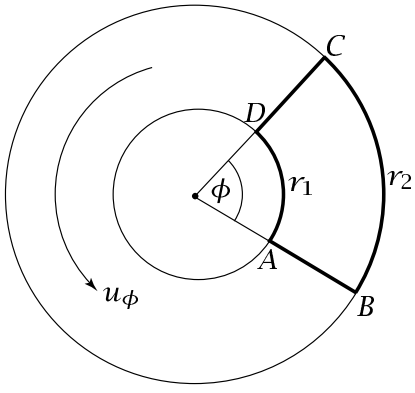

Fig. 4.1 Evaluation of circulation in the axi-symmetric vr vortex. The circulation around the path A–B–C–D is zero. This result does not depend on the radii r_1 or r_2 or the angle ϕ, and the circulation around any infinitesimal path not enclosing the origin is zero. Thus the vorticity is zero everywhere except at the origin.

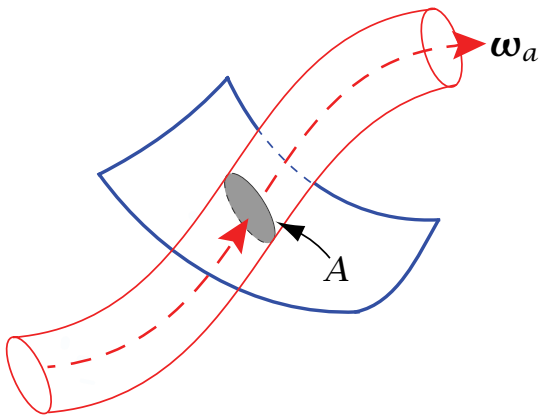

Fig. 4.2 A vortex tube passing through a material sheet. The circulation is the integral of the velocity around the boundary of A, and is equal to the integral of the normal component of vorticity over A.

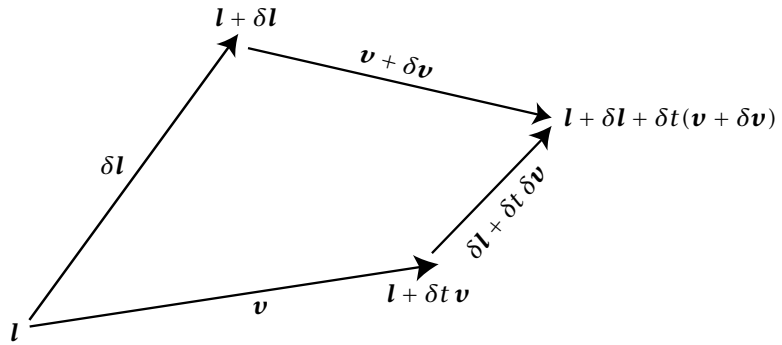

Fig. 4.3 Evolution of an infinitesimal material line $\delta\boldsymbol{l}$ from time t to time $t + \delta t$. It can be seen from the diagram that $\mathrm{D}\delta\boldsymbol{l}/\mathrm{D}t = \delta\boldsymbol{v}$.

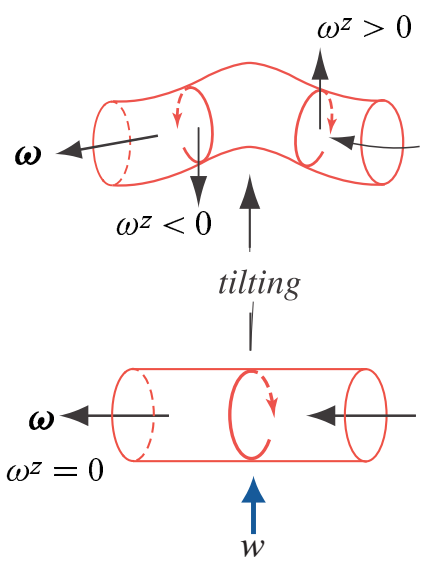

Fig. 4.4 The tilting of vorticity. Suppose that the vorticity, $\boldsymbol{\omega}$ is initially directed horizontally, as in the lower figure, so that ω^z, its vertical component, is zero. The material lines, and therefore also the vortex lines, are tilted by the postive vertical velocity W, thus creating a vertically oriented vorticity. This mechanism is important in creating vertical vorticity in the atmospheric boundary layer (and, one may show, the β-effect in large-scale flow).

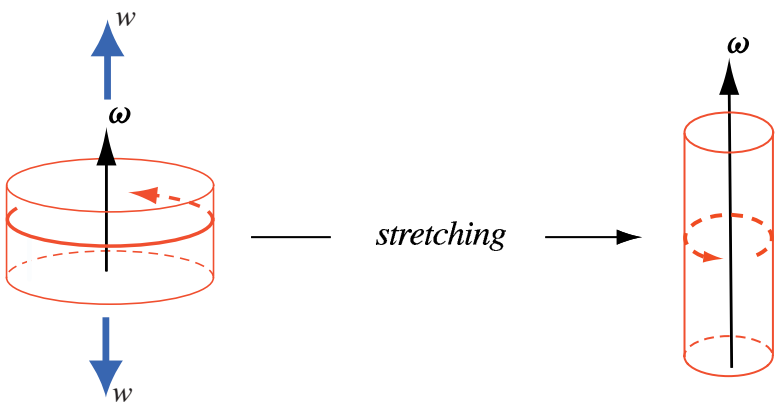

Fig. 4.5 Stretching of material lines distorts the cylinder of fluid as shown. Vorticity is tied to material lines, and so is amplified in the direction of the stretching. However, because the volume of fluid is conserved, the end surfaces shrink, the material lines through the cylinder ends converge and the integral of vorticity over a material surface (the circulation) remains constant, as discussed in section 4.3.2.

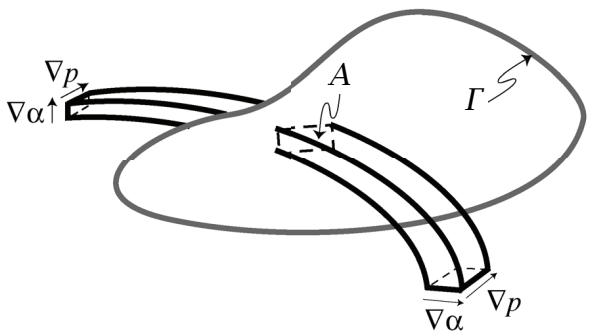

Fig. 4.6 Solenoids and the circulation theorem. Solenoids are tubes perpendicular to both $\nabla\alpha$ and ∇p, and they have a non-zero cross-sectional area if isolines of α and p do not coincide. The rate of change of circulation over a material surface is given by the sum of all the solenoidal areas crossing the surface. If $\nabla\alpha \times \nabla p = 0$ there are no solenoids.

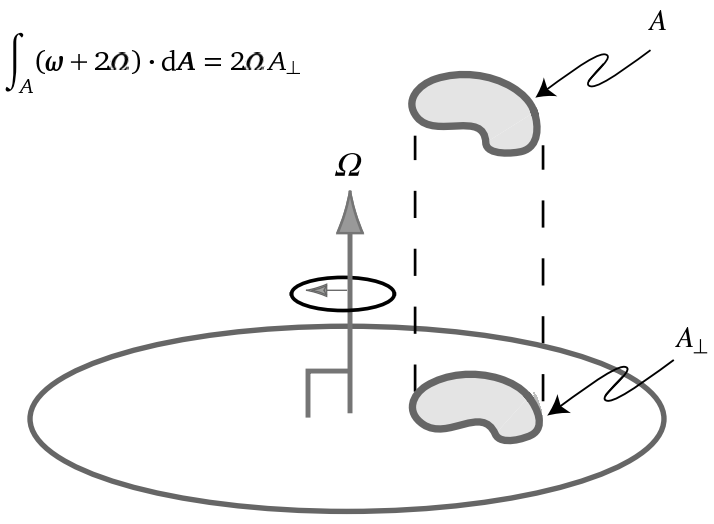

Fig. 4.7 The projection of a material circuit on to the equatorial plane. If a fluid element moves poleward, keeping its orientation to the local vertical fixed (e.g., it stays horizontal) then the area of its projection on to the equatorial plane increases. If its total (absolute) circulation is to be maintained, then the vertical component of the relative vorticity must diminish; that is, $\int_A (\boldsymbol{\omega} + 2\boldsymbol{\Omega}) \cdot \mathrm{d}\boldsymbol{A} = \int_A (\zeta + f)\,\mathrm{d}A =$ constant. Thus, the β term in $\mathrm{D}(\zeta + f)/\mathrm{D}t = \mathrm{D}\zeta/\mathrm{D}t + \beta v = 0$ ultimately arises from the *tilting* of a parcel relative to the axis of rotation as it moves meridionally.

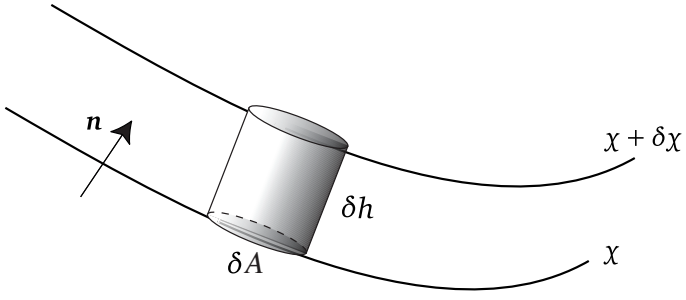

Fig. 4.8 An infinitesimal fluid element, bounded by two isosurfaces of the conserved tracer χ. As $\mathrm{D}\chi/\mathrm{D}t = 0$, then $\mathrm{D}\delta\chi/\mathrm{D}t = 0$.

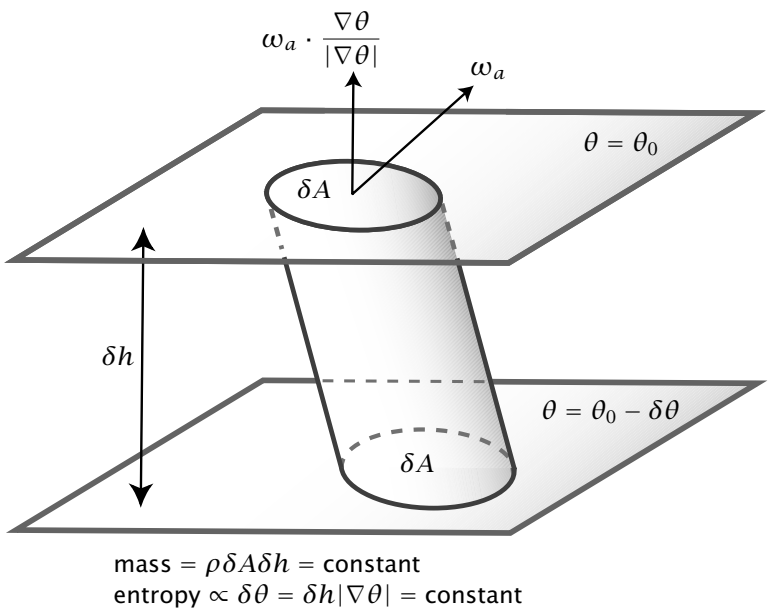

Fig. 4.9 Geometry of potential vorticity conservation. The circulation equation is $\mathrm{D}[(\boldsymbol{\omega}_a \cdot \boldsymbol{n})\delta A]/\mathrm{D}t = \boldsymbol{S} \cdot \boldsymbol{n}\,\delta A$, where $\boldsymbol{S} \propto \nabla\theta \times \nabla T$. We choose $\boldsymbol{n} = \nabla\theta/|\nabla\theta|$, where θ is materially conserved, to annihilate the solenoidal term on the right-hand side, and we note that $\delta A = \delta V/\delta h$, where δV is the volume of the cylinder, and the height of the column is $\delta h = \delta\theta/|\nabla\theta|$. The circulation is $C \equiv \boldsymbol{\omega}_a \cdot \boldsymbol{n}\,\delta A = \boldsymbol{\omega}_a \cdot (\nabla\theta/|\nabla\theta|)(\delta V/\delta h) = [\rho^{-1}\boldsymbol{\omega}_a \cdot \nabla\theta](\delta M/\delta\theta)$, where $\delta M = \rho\,\delta V$ is the mass of the cylinder. As δM and $\delta\theta$ are materially conserved, so is the potential vorticity $\rho^{-1}\boldsymbol{\omega}_a \cdot \nabla\theta$.

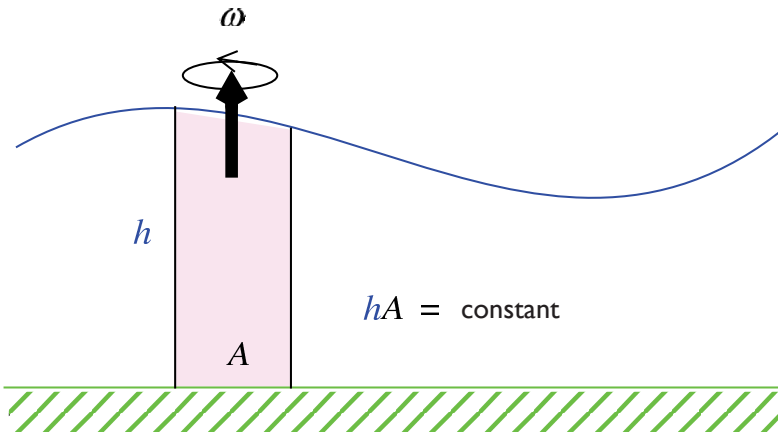

Fig. 4.10 The mass of a column of fluid, hA, is conserved in the shallow water system. Furthermore, the vorticity is tied to material lines so that ζA is also a material invariant, where $\zeta = \boldsymbol{\omega} \cdot \mathbf{k}$ is the vertical component of the vorticity. From this, ζ/h must be materially conserved; that is, $\mathrm{D}(\zeta/h)/\mathrm{D}t = 0$, which is the conservation of potential vorticity in a shallow water system. In a rotating system this generalizes to $\mathrm{D}[(\zeta + f)/h]/\mathrm{D}t = 0$.

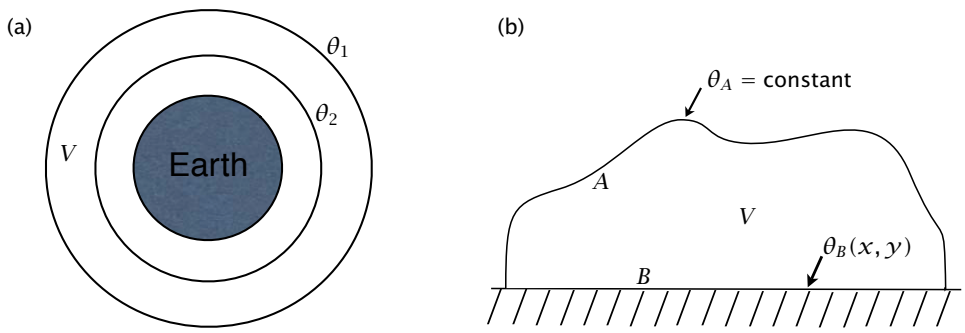

Fig. 4.11 (a) Two isentropic surfaces that do not intersect the ground. The integral of PV concentration over the volume between them, V, is zero, even if there is heating and the contours move. (b) An isentropic surface, A, intersects the ground, B, thus enclosing a volume V. The rate of change of PV concentration over the volume is given by an integral over B.

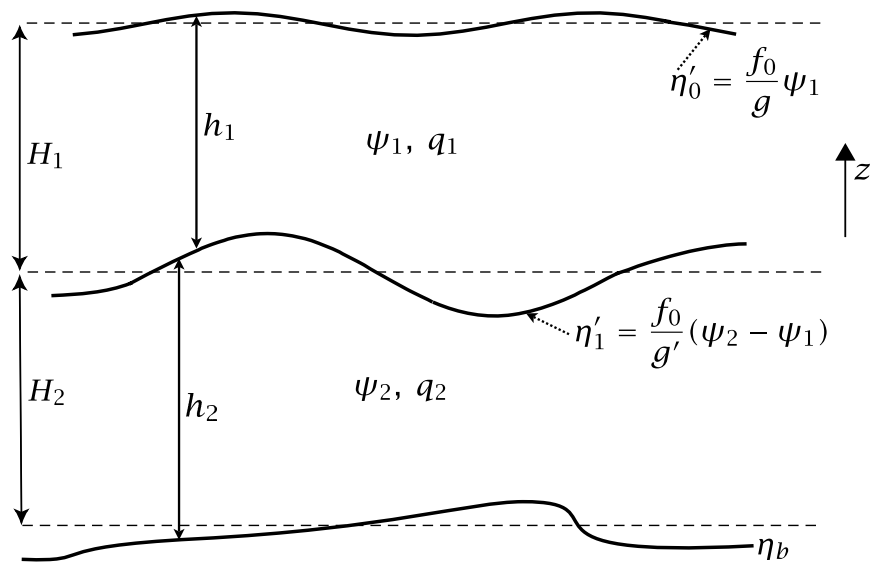

Fig. 5.1 A quasi-geostrophic fluid system consisting of two immiscible fluids of different density. The quantities η' are the interface displacemens from the resting basic state, denoted with dashed lines, with η_b being the bottom topography.

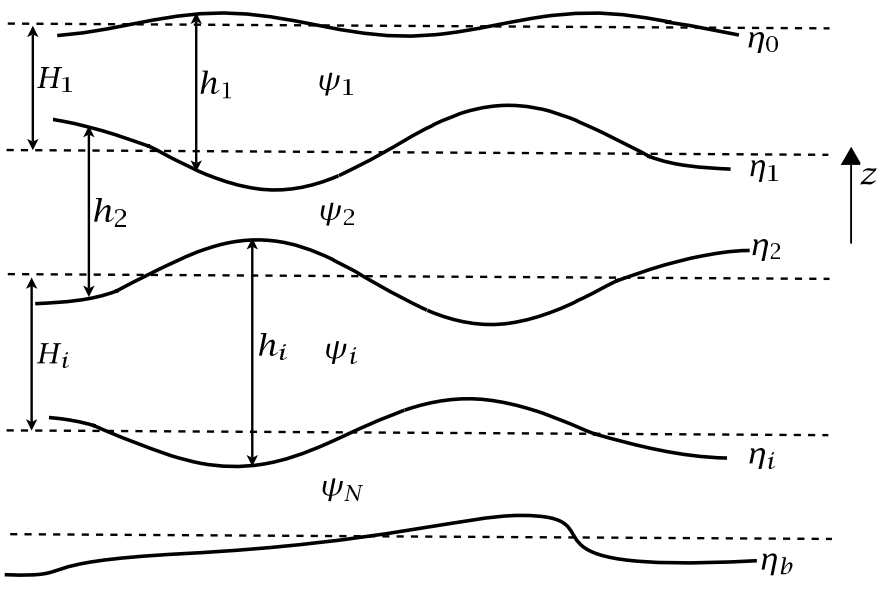

Fig. 5.2 A multi-layer quasi-geostrophic fluid system. Layers are numbered from the top down, i denotes a general interior layer and N denotes the bottom layer.

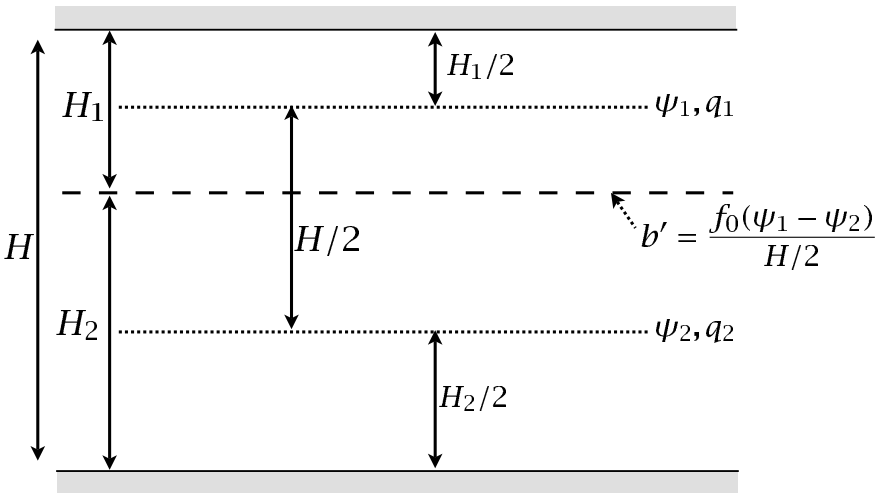

Fig. 5.3 The two-level quasi-geostrophic system with a flat bottom and rigid lid at which $w = 0$.

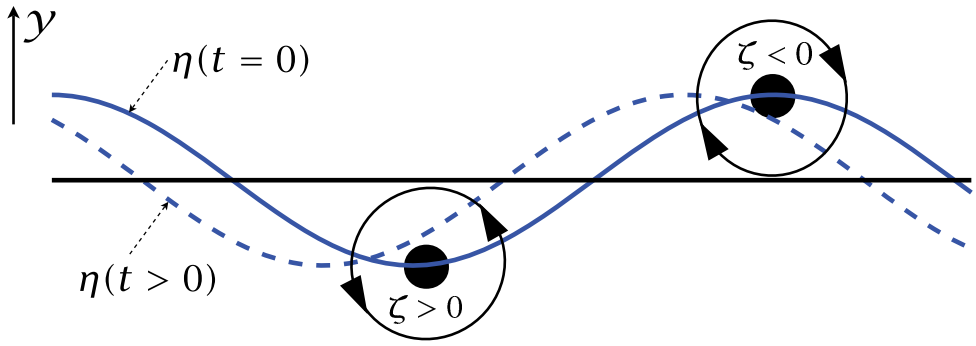

Fig. 5.4 The mechanism of a two-dimensional (x-y) Rossby wave. An initial disturbance displaces a material line at constant latitude (the straight horizontal line) to the solid line marked $\eta(t = 0)$. Conservation of potential vorticity, $\beta y + \zeta$, leads to the production of relative vorticity, as shown for two parcels. The associated velocity field (arrows on the circles) then advects the fluid parcels, and the material line evolves into the dashed line. The phase of the wave has propagated westwards.

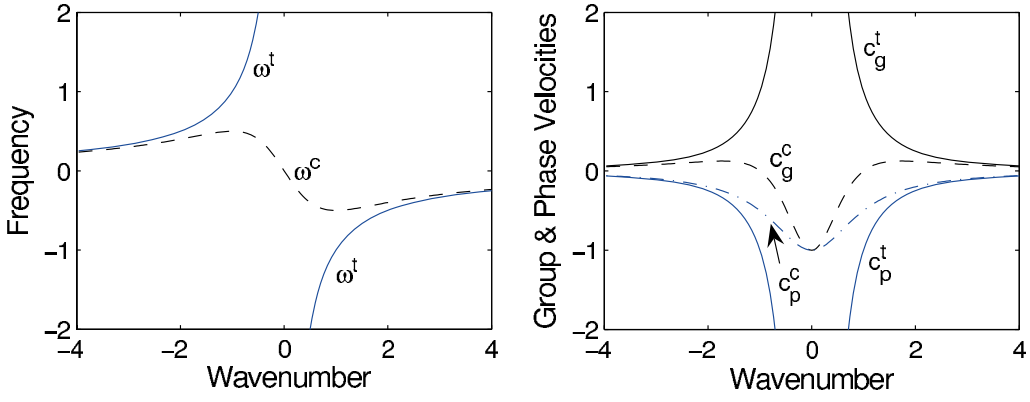

Fig. 5.5 Left: the dispersion relation for barotropic (ω^t, solid line) and baroclinic (ω^c, dashed line) Rossby waves in the two-layer model, calculated using (5.192) and (5.193) with $k^y = 0$, plotted for both positive and negative zonal wavenumbers and frequencies. The wavenumber is non-dimensionalised by k_d, and the frequency is non-dimensionalized by β/k_d. Right: the corresponding zonal group and phase velocities, $c_g = \partial\omega/\partial k^x$ and $c_p = \omega/k^x$, with superscript 't' or 'c' for the barotropic or baroclinic mode, respectively. The velocities are non-dimensionalized by β/k_d^2.

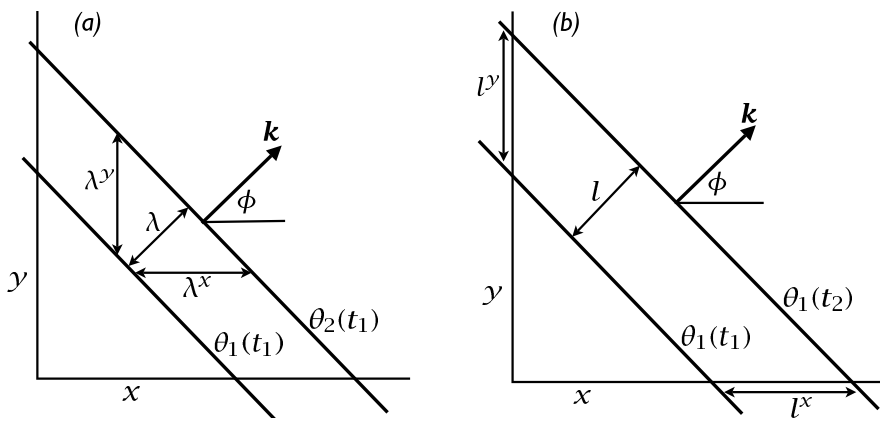

Fig. 5.6 The propagation of a two-dimensional wave. (a) Two lines of constant phase (e.g., two wavecrests) at a time t_1. The wave is propagating in the direction $\boldsymbol{k}$ with wavelength λ. (b) The same line of constant phase at two successive times. The phase speed is the speed of advancement of the wavecrest in the direction of travel, and so $c_p = l/(t_2 - t_1)$. The phase speed in the x-direction is the speed of propagation of the wavecrest along the x-axis, and $c_p^x = l^x/(t_2 - t_1) = c_p/\cos\phi$.

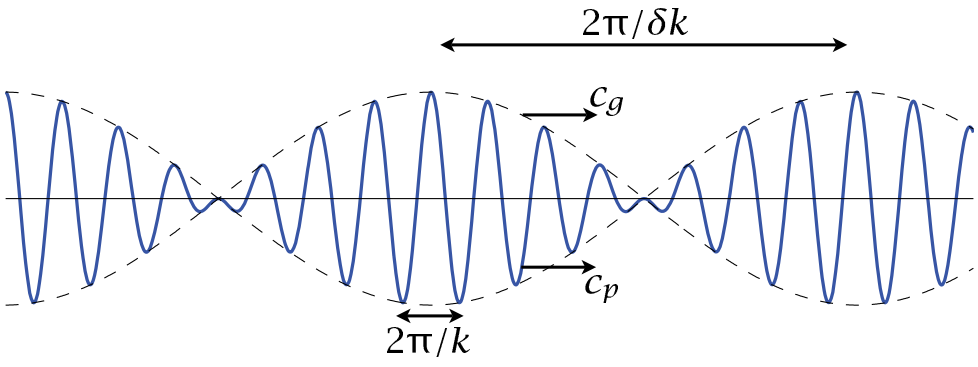

Fig. 5.7 Superposition of two sinusoidal waves with wavenumbers k and $k + \delta k$, producing a wave (solid line) that is modulated by a slowly varying wave envelope or wave packet (dashed line). The envelope moves at the group velocity, $c_g = \partial\omega/\partial k$ and the phase of the wave moves at the group speed $c_p = \omega/k$.